INFLUENCE OF THE JET VELOCITY PROFILE ON FLOW CHARACTERISTICS NEAR AN OBSTACLE

A. I. Abrosimov

UDC 532.526

The flow of a submerged jet pulsating along the normal in a plane obstacle is considered provisionally to consist of two domains [1]: in the first, starting with the nozzle exit the flow is propagated according to free shear flow regularities; the second, located between the section where the influence of the obstacle is felt noticeably and the wall, is the so-called interaction domain (I and II in Fig. 1). In turn, this latter consists of the turning zone enclosing the near-wall flow with negative pressure gradient and the fan semibounded jet for the axisymmetric problem.

Both the characteristic turbulence and the average velocity profile [2] vary downstream in a free submerged jet. Among the known factors influencing the characteristics of a jet issuing into the interaction domain are the velocity distribution in the initial section, the near-wall boundary layer parameters at the nozzle wall, the initial turbulence (intensity and scale of turbulent perturbations), the distance between the nozzle and the obstacle $H = h/d$, etc. ($d = 2r_0$ is the nozzle diameter).

Analysis shows that the near-wall boundary layer on an obstacle is developed under small Reynolds numbers conditions $Re_m = u_m\delta/\nu$ and $Re^{**} = u_m\delta^{**}/\nu$, where u_m is the velocity on the outer boundary of the near-wall boundary layer, δ is the layer thickness, and δ^{**} is the thickness of the loss of momentum. For example, for a jet with a rectangular initial velocity profile and low turbulence intensity at the nozzle exit ($\varepsilon \leq 0.01$) and a distance $R = r/d = 1.25$ in the radial direction from the critical point of the obstacle in the mode $Re = V_0 d/\nu = 11{,}000$, $Re^{**} = 45$, while $Re^{**} = 150$ in the mode $Re = 10^5$ (V_0 is the mean mass velocity at the nozzle exit). Starting from existing representations, the influence of stream turbulence at the input in the interaction domain should also be expected for relatively small distances from the critical point of the obstacle, in addition to the spreading jet velocity profile on the structure of the near-wall boundary layer. In connection with the development of methods of intensifying jet heat and mass transport processes the study of the influence of each of the noted factors separately is urgent.

It is shown in [3, 4] that the passage from a rectangular initial velocity profile in a laminar jet pulsating on an obstacle to a parabolic profile results in substantial intensification of the heat transport in the neighborhood of the obstacle critical point. This increase is almost double for a circular jet [4].

The influence of the average velocity profile characteristic for free isothermal submerged jets on certain near-wall boundary layer characteristics on a plane obstacle is investigated in this paper.

The flow diagram is represented in Fig. 1. It is assumed that the flow intrinsic to a free submerged jet holds in domain I while the flow is laminar in II. The flow in the interaction domain is studied. The Navier–Stokes and continuity equations for an incompressible fluid were converted into the system [5]

$$-\frac{\partial}{\partial X}\left(\frac{1}{R}\frac{\partial\bar{\psi}}{\partial X}\right)-\frac{\partial}{\partial R}\left(\frac{1}{R}\frac{\partial\bar{\psi}}{\partial R}\right)-\bar{\omega}=0,$$

$$R^2\left[\frac{\partial}{\partial X}\left(\frac{\bar{\omega}}{R}\frac{\partial\bar{\psi}}{\partial R}\right)-\frac{\partial}{\partial R}\left(\frac{\bar{\omega}}{R}\frac{\partial\bar{\psi}}{\partial X}\right)\right]-\frac{\partial}{\partial X}\left[R^3\frac{\partial\left(\frac{1}{\mathrm{Re}}\frac{\bar{\omega}}{R}\right)}{\partial X}\right]-\frac{\partial}{\partial R}\left[R^3\frac{\partial\left(\frac{1}{\mathrm{Re}}\frac{\bar{\omega}}{R}\right)}{\partial R}\right]=0,$$

by using the variable vorticity ($\omega = \partial u/\partial x - \partial v/\partial r$) and stream functions ($\partial\psi/\partial x = -ur$, $\partial\psi/\partial r = vr$), where $X = x/d$, $R = r/d$, $\bar{\omega} = \omega d/V_0$; $\bar{\psi} = \psi/(d^2V_0)$

Istra. Translated from Zhurnal Prikladnoi Mekhaniki i Tekhnicheskoi Fiziki, No. 6, pp. 85-92, November-December, 1988. Original article submitted July 1, 1987.

0021-8944/88/2906-0842 $12.50

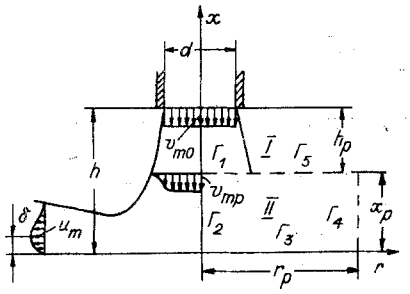

Fig. 1

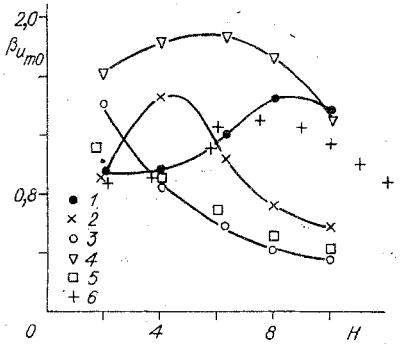

Fig. 2

The computational domain was bounded by the obstacle, the plane of the beginning of the interaction domain standing a distance $X_p = x_p/d = 1 + 0.05H$ off from the obstacle, and a cylindrical surface of radius $R_p = r_p/d = 2 + 0.1H$. The relationship for X_p is obtained according to experimental results [6, 7]. The base of the size of the computational domain in the radial direction is performed in [8] with the increase in the stream turning domain taken into account as the obstacle recedes from the nozzle and also from the condition of insignificant change in the calculation results in the gradient flow domain as R_p grows relative to the quantity obtained by the formula presented.

The average velocity distribution in the free jet was given by using the P-function [9]

$$\frac{v}{v_{m0}} = \frac{1}{2\xi}\exp\left(-\frac{r^2}{4\xi}\right)\int_0^{r_0}\exp\left(-\frac{\rho^2}{4\xi}\right) I_0\frac{(\rho r)}{2\xi}\rho d\rho.$$

Here I_0 is the zero-order Bessel function of imaginary argument, v_{m0} is the velocity on the axis in the jet initial section, and the P-function is tabulated in [10]. This relationship permits description of the continuous deformation of the velocity profile from the original, for instance, rectangular profile, to a Gaussian one far downstream.

If $H_p = H_i$ (H_i is the length of the jet initial section), then according to [10] $\sqrt{\xi}/r_0 = 0.18$. In the domain $\leqslant = H_p \leqslant H_i$ the change in $\sqrt{\xi}/r_0$ is described by the approximate dependence $\sqrt{\xi}/r_0 = 0.18H_p/H_i$ ($H_p = H - X_p$) [11]. In the transition and main sections of the jet $\sqrt{\xi}/r_0$ was determined from P-function tables by using experimental data on the velocity change along the axis.

The efflux conditions for the jets investigated and the values of the axial velocity at the entrance to the computational domain for the considered distances between the nozzle exit and the obstacle are presented in Table 1.

Values of the velocity for each node of the computational mesh were found at the entrance to the interaction domain (see Fig. 1, boundary Γ1) by means of the value obtained for $\sqrt{\xi}/r_0$ and the P-function tables. On the axis (the boundary Γ2) symmetry conditions ($\overline{\psi} = \partial\overline{\omega}/\partial R = 0$) are satisfied. The boundary Γ3 is the obstacle surface. From the attachment and impermeability conditions of the wall $\overline{\psi} = 0$. The vorticity at the axis and on the wall was calculated from approximate formulas of second order of accuracy [5]. The stream characteristics along the direction of motion vary comparatively slowly at the exit from the computational domain (the boundary Γ4) $\partial\overline{\psi}/\partial R = \partial\overline{\omega}/\partial R = 0$. The stream on the boundary Γ5 is considered nonvortical ($\overline{\omega}/R = \partial\overline{\psi}/\partial X = 0$). The problem was solved numerically by a finite-difference method [5].

The computational 23 × 23 mesh had condensation near the wall and in the radical direction near R = 0.5. Within the near-wall boundary layer 7-9 points of the computational mesh were found arranged according to a geometric progression. Preliminary computations showed that the thickness of the near-wall boundary layer near the axis is $\overline{\delta}_0 = \delta_0/d \sim \mathrm{Re}^{-0.38}$. The distance from the wall to the nearest series of the mesh varied in proportion to $\overline{\delta}_0$ and was $7\cdot10^{-4}$d for Re = 11,000, for instance. The mesh series closest to the axis was 0.1 d removed. The relationship

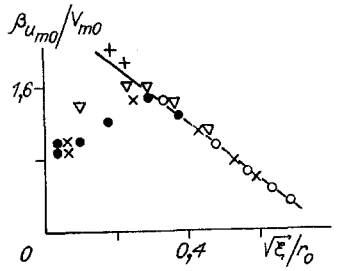

Fig. 3

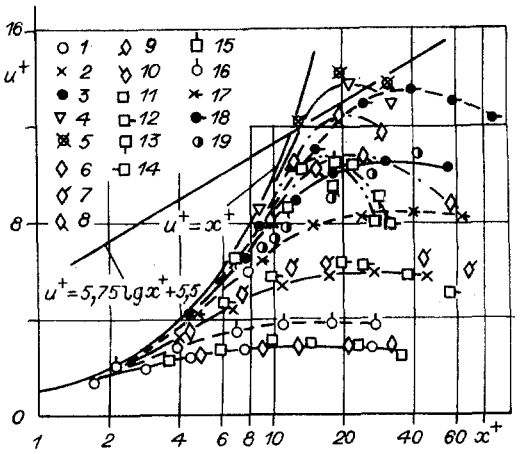

Fig. 4

$$\left(\frac{\varphi^n-\varphi^{n-1}}{\varphi^{n-1}_{\max}}\right)_{\max}\leqslant 10^{-3},$$

where φ is a variable, and n is the number of the iteration, was used as the convergence criterion for the iteration process of solving the boundary value problem; the subscript max denotes the greatest value in the field of variables.

The change in the velocity gradient near the axis $\beta_{u_{m0}} = (\partial u_m/\partial r)_{r=0} d/V_0$ is shown in Fig. 2 for different jet efflux conditions as a function of the distance H. For a rectangular velocity profile at the nozzle exit and $\varepsilon \leq 0.01$ (points 1) $\beta_{u_{m0}}$ to H = 4 is increased insignificantly, grows more intensively later and reaches the maximal value at $H \approx 8.5$, i.e., when the beginning of the interaction domain is at the end of the jet transition section. It should be noted that since the flow was assumed laminar in the computational flow domain, then the change in $\beta_{u_{m0}}$ at the distance $H_p = H_i$ is caused only by velocity profile deformation, and in the transition to the same, by velocity diminution on the axis.

As the initial turbulence increases (points 2 and 3 correspond to $\varepsilon = 0.093$; 0.209), in order to keep the velocity profile rectangular at the nozzle exit, the distance H where $\beta_{u_{m0}} = (\beta_{u_{m0}})_{\max}$ shifts to the domain of smaller values. Here $(\beta_{u_{m0}})_{\max}$ is almost independent of ε. For $\varepsilon = 0.209$ the change in $\beta_{u_{m0}}$ with the increase in H is characterized by a monotonic diminution. Measurements [15] (the points 6) performed for a jet with rectangular initial velocity profile for $\varepsilon \leq 0.01$ are in good agreement with the computation to H = 5. Lowering of the experimental values of $\beta_{u_{m0}}$ in the domain H > 5 is visibly associated with the more rapid jet dissipation than was assumed in the computations. A comparison with data referring to an artificially turbulized jet ($\varepsilon = 0.22$) with a rectangular velocity profile at the nozzle exit [16] (points 5) shows that the agreement is good in the domain H = 4-10; however, the computed data at H = 2 exceed experiment by almost 25%.

TABLE 1

Initial velocity profile	ε	v_{mp}/v_{m_0} at H = 2	H = 4	H = 6,3	H = 8	H = 10	Source
Rectangular	0,01	1	1	1	0,95	0,83	[12]
»	0,093	1	0,982	0,741	0,59	0,511	[12]
»	0,209	0,89	0,662	0,524	0,457	0,408	[12]
Developed turublent	0,02	1	0,991	0,949	0,854	0,709	[13]
Parabolic, laminar jet	—	0,9993	0,9982	0,9964	0,9952	0,9938	[14]

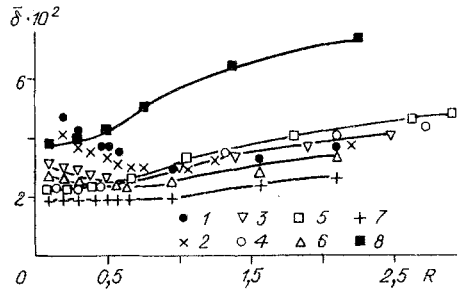

Fig. 5

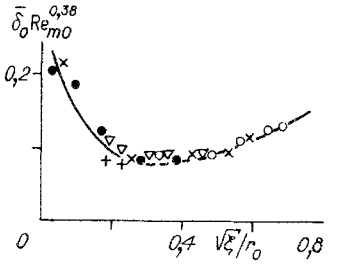

Fig. 6

As the taper of the velocity profile increases in the jet initial section, the velocity gradient $\beta_{u_{m0}}$ grows in the $2 \le H \le 10$ range. For a developed turbulent initial velocity profile and $\varepsilon \approx 0.02$ the maximum value of $\beta_{u_{m0}}$ (points 4) is observed at $H \approx 5.5$. For a laminar impact jet with parabolic initial velocity profile in the range of H investigated, the value of $\beta_{u_{m0}}$ remains approximately constant and exceeds the gradient for a jet with rectangular initial velocity profile at H = 2 by approximately four times for $\varepsilon \le 0.01$.

For a turbulent impact jet with rectangular initial velocity profile for $\varepsilon \le 0.01$, the following relationships for the occupation of $\beta_{u_{m0}}$ can be recommended:

$$\beta_{u_{m0}} = 0.95 = \text{const} \quad \text{for } H = 2-4,$$
$$\beta_{u_{m0}} = 0.48 + 0.118H \quad \text{for } H = 4-8.5,$$
$$\beta_{u_{m0}} = 2.59 - 0.129H \quad \text{for } H = 8.5-12.$$

For impact jets with rectangular initial velocity profile and different turbulence intensity at the nozzle exit the values of $\beta_{u_{m0}}/V_{m0}$ as a function of $\sqrt{\xi}/r_0$ are grouped around one curve characterized by a maximum at approximately $\sqrt{\xi}/r_0 = 0.3$ (Fig. 3, the notation of the points is analogous to Fig. 2). Here $V_{m0} = v_{m0}/V_0$. As $\sqrt{\xi}/r_0$ grows in the range 0.03-0.3 the velocity gradient increases $(\beta_{u_{m0}}/V_{m0})_{max} = 1.55$. For a developed turbulent initial velocity profile the position of the maximum and its magnitude remain almost the same for $\varepsilon \approx 0.02$. No maximum is observed for a parabolic initial velocity profile.

In the domain $\sqrt{\xi}/r_0 \ge 0.3$ computed points with insignificant deviation are plotted on the line $\beta_{u_{m0}}/V_{m0} = 2.41-3.09\sqrt{\xi}/r_0$ (Fig. 3) for all the regimes investigated. This dependence is conserved even in the domain $\sqrt{\xi}/r_0 < 0,3$ in the case of a parabolic velocity profile at the nozzle exit.

The distribution of the velocity gradient $\beta_{u_m} = (\partial u_m/\partial r)d/V_0$ in the radial direction has a number of singularities. In an impact jet with rectangular initial velocity profile for $\varepsilon \le 0.01$ first β_{u_m} grows at H = 2 with distance from the axis, reaches a maximal value at $R \approx 0.56$ and then diminishes to zero at the end of the gradient flow domain ($R \approx 1.0$). The maximal value of the velocity gradient $(\beta_{u_m})_{max}$ is approximately 1.8 times greater than at the axis. As the obstacle recedes from the nozzle, the ratio $(\beta_{u_m})_{max}/\beta_{u_{m0}}$ diminishes somewhat and the peak itself shifts to the axis. At $H \ge 8$ the maximal value β_{u_m} is on the axis.

As the initial turbulence intensity increases reconstruction of the velocity profile of a spreading jet occurs more rapidly; consequently, in an impact jet with $\varepsilon = 0.093$ the peripheral peak in the radial distribution β_{u_m} is observed only at $H \le 4$ while in the regime with $\varepsilon = 0.209$ the location of $(\beta_{u_m})_{max}$ agrees with the axis starting with H = 2.

As a jet with a developed turbulent velocity profile at the nozzle exit spreads on the obstacle for $\varepsilon \approx 0.02$ the distribution of u_m at small H also has an inflection point and the curve $\beta_{u_m} = f(R)$ is characterized by a peripheral maximum. Under these conditions

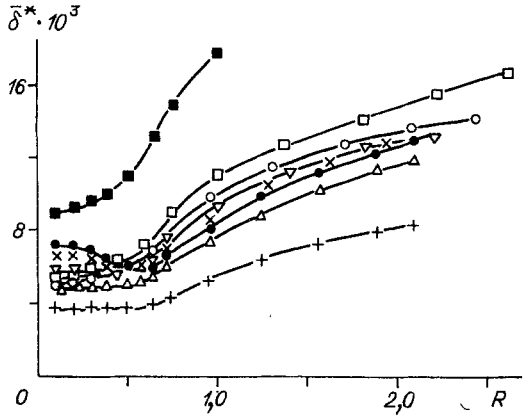

Fig. 7

the peak is not large and holds only at $H \leq 4$. At $H = 2$ the ratio is $(\beta_{u_m})_{max}/\beta_{u_{m0}} \approx 1.18$ and the peak is at $R \approx 0.3$.

In an impact laminar jet with parabolic initial velocity profile the distribution $\beta_{u_m} = f(R)$ has a bell-shape with $(\beta_{u_m})_{max}$ on the axis for all the H investigated.

The longitudinal velocity profile $u^+ = u/u_*$ near the wall is represented in Fig. 4 for Re = 11,000 and different velocity distributions in the jet at the entrance to the interaction domain ($u_* = \sqrt{\tau_w/\rho}$ is the friction velocity and $x^* = u_* x/\nu$). Points 1-15 refer to a rectangular initial jet velocity profile for $\varepsilon \leq 0.01$: 1-5 are calculated for H = 2; 6-10 for 3, and 11-15 for 10).

In the gradient and transition flow domains of a fan jet the velocity profile in the near-wall boundary layer is not self-similar. The layer thickness with a linear change in the velocity increases with distance from the obstacle critical point (points 1 refer to the section at R = 0.1064; 2 to 0.4446; 3 to 0.949; 4 to 1.89; 5 to 2.11). Let us note that at H = 2 the gradient zone is terminated approximately at R = 1.0, while the transition zone extends approximately to R = 2.5. The curves $u^+ = f(x^+)$ have humps due to the presence of a velocity maximum at the outer boundary of the near-wall boundary layer. The deviation of the velocity distribution from the linear dependence is caused by the transition of the near-wall boundary layer into the external flow for small R (gradient flow) and in the jet boundary layer of a fan jet. This deviation is already noticeable at $x^+ = 1$ for R = 0.1064 and approximately at $x^+ = 8$ for R = 1.8. The computed data agree qualitatively with results of experiments [17] (points 19 to $Re = 1.61 \cdot 10^5$, H = 11.8 and R = 3.25).

The velocity distribution in a near-wall boundary layer varies weakly as the obstacle recedes from the nozzle at fixed R and unchanged jet efflux conditions (point 16 to R = 0.1064; 7 to 0.446; 8 to 1.034; 9 to 1.84; 10 to 2.63; 11 to 0.1064; 12 to 0.4446; 13 to 1.01; 14 to 1.82; 15 to 2.63). The influence of H is especially small in the gradient flow zone.

The passage from a rectangular initial velocity profile for $\varepsilon \leq 0.01$ to a parabolic (the points 16 to R = 0.1064; 17 – 0.4446; 18 – 0.949, H = 2) is accompanied by expansion of the layer with a linear change in velocity and shift of the curve into the domain of large values of u^+ for the same R. The position of the maximum of the dependence $u^+ = f(x^+)$ governing the boundary of the near-wall boundary layer is in the range $x^+ = 10$-40.

The thickness $\bar{\delta} = \delta/d$ of the near-wall boundary layer in the domain $R \geqslant 0.1$ was determined from the graph of the radial velocity $u = f(x)$ constructed from velocity values at the nodes of the computational mesh. The boundary layer thickness $\bar{\delta}_0^*$ near the axis was found by two methods: by extrapolation of the curve $\bar{\delta} = f(R)$ to the axis in the domain $R < 0.1$ and by the graph of the change in the axial velocity gradient $\beta_{v_m} = (\partial v_m/\partial x)d/V_0 = f(x)$ under the assumption that the coordinate corresponding to $(\beta_{v_m})_{max}$ is the outer boundary of the near-wall layer. Both methods yielded similar results.

The velocity profile of a spreading jet exerts strong influence on not only $\bar{\delta}$ but also on the nature of its change in a radial direction (Fig. 5, Re = 11,000). For a rectangular initial velocity profile for $\varepsilon \leq 0.01$ (the points 1 are H = 2; 2 – 4; 3 – 6.3; 4 – 8; 5 – 10) at H = 10 when the flow transition in the jet to the self-similar is basically terminated, the boundary layer thickness grows monotonically with distance from the critical point of the obstacle. If the distance H is shortened, then singularities appear in the radial distribution of $\bar{\delta}$. At H = 6.3, when $H_p \approx H_i$ and therefore, the beginning of the interaction domain agrees with the boundary of the jet initial section ($H_i = 5$), δ diminishes with distance from the critical point in the domain $0.1 \leq R \leq 0.5$. At $R \approx 0.5$ it achieves the minimal value and grows smoothly with further displacement downstream. Diminution of the distance between the nozzle and the obstacle in the $H < 6.3$ range accompanied by expansion of the plane section in the velocity profile of the spreading jet results in an increase in $\bar{\delta}_0$ and a shift of the radial coordinate corresponding to $\bar{\delta}_{min}$ downstream. At H = 2 this coordinate is found approximately at R = 1.0.

At H = 2 the boundary layer becomes thinner with the transition from the rectangular initial velocity profile of the jet for $\varepsilon \leq 0.01$ to the developed turbulent profile; for $\varepsilon \approx 0.02$ the trough in the distribution $\bar{\delta} = f(R)$ diminishes and the coordinate corresponding to $\bar{\delta}_{min}$ shifts to the axis (point 6, H = 2). For a parabolic initial velocity profile at H = 2 (points 7) the near-wall boundary layer thickness is approximately constant up to R = 0.9 and later gradually increases downstream. Let us note that in a highly turbulized ($\varepsilon = 0.209$) impact jet (points 8) the value of $\bar{\delta}$ is approximately 1.7 times greater at H = 10 than in a jet with a low ($\varepsilon \leq 0.01$) turbulence intensity at the nozzle exit.

A computation of the boundary layer thickness $\bar{\delta}_0$ by means of the relationship $\bar{\delta}_0 = 1.95/(\beta_{u_{m0}}\mathrm{Re})^{0.5}$ constructed on the basis of the Homan solution [18] with values of $\beta_{u_{m0}}$ obtained in this paper substituted for a jet with a rectangular initial velocity profile for $\varepsilon \leq 0.01$ yields a lowering of $\bar{\delta}_0$ of 1.6-2.5 times, as compared with the data in Fig. 5, in the range of H from 2 to 10. An analogous discrepancy was detected also in the tests [19] where it is noted that the measured boundary layer thickness is higher by 50-100% than that calculated by the formula presented.

Results on the change in the near-wall boundary layer thickness near the axis are represented in Fig. 6 (notation corresponds to Fig. 2). It can be seen that the results of the computations in the variables $\bar{\delta}_0\mathrm{Re}_{m0}^{0.38}$ and $\sqrt{\bar{\xi}}/r_0$ are grouped around one curve having a minimum at $\sqrt{\bar{\xi}}/r_0 \approx 0.3$. The left side of the curve ($0.03 \leq \sqrt{\bar{\xi}}/r_0 \leq 0.3$) is described by the relationships $\bar{\delta}_0\mathrm{Re}_{m0}^{0.38} = 0.082 + 1.66\,(0.3 - \sqrt{\bar{\xi}}/r_0)^{1.89}$ while the right side ($\sqrt{\bar{\xi}}/r_0 \geq 0.3$) is described by the relationship $\bar{\delta}_0\mathrm{Re}_{m0}^{0.38} = 0.082 + 0.3\,(\sqrt{\bar{\xi}}/r_0 - 0.3)^{1.89}$. These curves are superposed in Fig. 6. Here $\mathrm{Re}_{m0} = v_{m0}d/\nu$.

At H = 2 the displacement thickness $\bar{\delta}^* = \delta^*/d$ (Fig. 7, Re = 11,000, the notation corresponds to Fig. 5) for a rectangular initial velocity profile and $\varepsilon \leq 0.01$ first diminishes with distance from the axis in the radial direction, reaches the minimal value $\bar{\delta}_{min}^*$ at $R \approx 0.55$ and later grows. The ratio $\bar{\delta}_0^*/\bar{\delta}_{min}^* = 1.23$. As the obstacle recedes from the nozzle, the trough in the radial distribution of $\bar{\delta}^*$ diminishes, it is almost unnoticed at H = 6.3 and at H = 8 the change in $\bar{\delta}^*$ is characterized by a smooth increase downstream. The section with the most-filled-in velocity profile ($\bar{\delta}^* = \bar{\delta}_{min}^*$) agrees with the section in which β_{u_m} has the greatest magnitude.

For a rectangular initial velocity profile for $\varepsilon = 0.093$ the trough in the distribution of $\bar{\delta}^*$ is observed only at H = 2. It is found at $R \approx 0.55$ and $\bar{\delta}_0^*/\bar{\delta}_{min}^* = 1.19$. For H = 2 and $\varepsilon = 0.209$ the displacement thickness increases smoothly with distance from the obstacle critical point.

The passage from the rectangular initial velocity profile for $\varepsilon \leq 0.01$ to a developed turbulent profile with $\varepsilon \approx 0.02$ and later to the parabolic profile at H = 2 is accompanied by a diminution of $\bar{\delta}^*$, where the displacement thickness at a distance $0.1 \leq R \leq 0.5$ in these regimes remains approximately constant and grows as R increases further. It is characteristic that near the axis $\bar{\delta}^*$ at H = 2 is almost two times smaller for a parabolic initial velocity profile than for a rectangular profile and $\varepsilon \leq 0.01$.

Processing the computational data on the displacement thickness near the axis showed that the change in the parameter $\bar{\delta}_0^*\mathrm{Re}_{m0}^{0.5}$ as a function of $\sqrt{\bar{\xi}}/r_0$ is subject to a single

dependence. The generalizing curve has a minimum at $\sqrt{\xi}/r_0 = 0.3$. In the domain $0.03 \leq \sqrt{\xi}/r_0 \leq 0.3$ it can be described by the formula $\overline{\delta}_0 * Re_{m0}^{0.5} = 0.52 + 2.63\,(0.3 - \sqrt{\xi}/r_0)^{1.77}$, while in the domain $\sqrt{\xi}/r_0 \geq 0.3$ the formula is $\overline{\delta}_0 * Re_{m0}^{0.5} = 0.52 + 1.62\,(\sqrt{\xi}/r_0 - 0.3)^{1.44}$.

Computations showed that the formparameter $\varkappa = \delta^*/\delta^{**}$ in all the efflux regimes and distances H considered increases with distance from the obstacle critical point, where the range of variation of $\varkappa$ with the growth of R diminishes as the regime parameters change and it can be taken in a first approximation that, for instance, a $\varkappa = 2.6$ at R = 1.8. At R = 0.1 the change in $\varkappa$ is successfully described by the relationship $\varkappa_{0.1} = 2.24(\sqrt{\xi}/r_0)^{0.029}$, which extends the data obtained with an error not exceeding 5%.

LITERATURE CITED

1. B. N. Yudaev, M. S. Mikhailov, and V. K. Savin, Heat Transfer during Jet Interaction with Obstacles [in Russian], Mashinostroenie, Moscow (1977).
2. G. N. Abramovich, S. Yu. Krashennikov, A. N. Sekundov, et al., Turbulent Mixing of Gas Jets [in Russian], Nauka, Moscow (1974).
3. E. M. Sparrow and L. Lee, "Analysis of the flow field and heat and mass transfer during impact of an inhomogeneous plane jet," Trans. ASME, Heat Transmission, 97, No. 2 [Russian translation] (1975).
4. A. I. Abrosimov, "On the question of the inner peak of the heat elimination coefficient on a plate bombarded by a perpendicular jet," Teplofiz. Vys. Temp., 22, No. 3 (1984).
5. A. D. Gosman, V. M. Pan, A. K. Ranchell, et al., Numerical Methods of Investigating Viscous Fluid Flows [Russian translation], Mir, Moscow (1972).
6. S. Beltaos and N. Rajaratnam, "Impinging circular turbulent jets," J. Hydraul. Div. Proc. Am. Soc. Civ. Eng., No. 10 (1974).
7. S. Beltaos and N. Rajaratnam, "Impingement of axisymmetric developing jets," J. Hydraul. Res., 15, No. 4 (1977).
8. S. I. Stepanov, "Axisymmetric jet interaction with a plane obstacle," Izv. Vyssh. Uchebn. Zaved., Mashinostr., No. 9 (1979).
9. A. N. Tikhonov and A. A. Samarskii, Equations of Mathematical Physics [in Russian], Gostekhizdat, Moscow (1953).
10. L. A. Vulis, Sh. A. Ershin, and L. P. Yarin, Principles of Gas Flame Theory [in Russian], Énergiya, Moscow (1968).
11. A. G. Prudnikov, M. S. Volynskii, and V. N. Sagalovich, Mixture-formation and Combustion Processes in Ramjet Engines [in Russian], Mashinostroenie, Moscow (1971).
12. G. S. Ginevskii, Theory of Turbulent Jets and Wakes [in Russian], Mashinostroenie, Moscow (1969).
13. R. Wille, "Beitrage fur Phanomenologie der Freistrahlen," Flugwiss., 11, No. 6 (1963).
14. G. W. Rankin and K. Sridhar, "Developing region of laminar jets with parabolic exit velocity profiles," Trans. ASME, J. Fluids Engng., 103, No. 6 (1981).
15. C. Donaldson and R. Snedeker, "A study of free jet impingement. Pt. 1. Mean properties of free and impinging jets," J. Fluid Mech., 45, No. 2 (1971).
16. E. P. Dyban, A. I. Mazur, and I. G. Davydenko, "Influence of turbulence on the longitudinal velocity gradient in the stagnation domain of impacting jets," Heat Transfer in Power Plants [in Russian], Naukova Dumka, Kiev (1978).
17. Porekh, Tsui, and Chermak, "Investigation of turbulent radial near-wall jet," Trans. ASME, J. Appl. Mech., 34, No. 2 [Russian translation] (1967).
18. H. Schlichting, Boundary Layer Theory [Russian translation], Nauka, Moscow (1974).
19. P. Hrycak, "Heat transfer from a row of impinging jets to concave cylindrical surfaces," Int. J. Heat Mass Transfer, 24, No. 3 (1981).